Computers in Biology and Medicine 109 (2019) 33–42

Contents lists available at ScienceDirect

Computers in Biology and Medicine

journal homepage: www.elsevier.com/locate/compbiomed

# Computer aided diagnosis for suspect keratoconus detection

Ikram Issarti[a,b,c,*], Alejandra Consejo[a,b,d], Marta Jiménez-García[a,b], Sarah Hershko[a,b], Carina Koppen[a,b], Jos J. Rozema[a,b]

[a] Department of Ophthalmology, Antwerp University Hospital (UZA), Edegem, Belgium
[b] Department of Medicine and Health Sciences, University of Antwerp, Antwerp, Belgium
[c] Applied Physics Research Team, Faculty of Sciences and Techniques of Tangier, Tangier, Morocco
[d] Institute of Physical Chemistry, Polish Academy of Sciences, Warsaw, Poland

ARTICLE INFO

*Keywords:*
Keratoconus suspect
Cornea
Machine learning
Computer aided diagnosis
Unstructured data
Mathematical modelling

ABSTRACT

*Purpose:* To develop a stable and low-cost computer aided diagnosis (CAD) system for early keratoconus detection for clinical use.

*Methods:* The CAD combines a custom-made mathematical model, a feedforward neural network (FFN) and a Grossberg-Runge Kutta architecture to detect clinical and suspect keratoconus. It was applied to retrospective data of *851* subjects for whom corneal elevation and thickness data was available. These data were divided into four groups: a control group (*312* eyes) with bilateral normal tomography, keratoconus suspect (*77* eyes) with a clinically diagnosed keratoconus in one eye and a normal fellow eye, mild keratoconus (*220* eyes), and moderate keratoconus (*229* eyes). The proposed framework is validated using 10-cross-validation, holdout validation and ROC curves.

*Results:* The CAD detects suspect keratoconus with an accuracy of *96.56%* (sensitivity *97.78%*, specificity *95.56%*) versus an accuracy of *89.00%* (sensitivity *83.00%*, specificity *95.00%*) for Belin/Ambrosio Deviation (BADD), and an accuracy of *79.00%* (sensitivity *58.00%*, specificity *99.70%*) for Topographical Keratoconus Classification (TKC). For the detection of mild to moderate keratoconus CAD shows nearly similar accuracies as previously described methods, with an average accuracy of *99.50%* for CAD, versus *99.46%* for BADD and *96.50%* for TKC. The proposed algorithm also provides a *70%* reduction in computation time, while increasing stability and convergence with respect to traditional machine learning techniques.

*Conclusion:* The proposed algorithm is highly accurate and provides a stable screening platform to assist ophthalmologists with the early detection of keratoconus. This framework could potentially be set up for any Scheimpflug tomography system.

## 1. Introduction

Keratoconus (KTC) is a non-infectious pathology that gradually deforms the cornea, the transparent structure at the front of the eye that focuses light through the lens on the retina. Healthy cornea has a convex aspherical shape and a large difference in refractive index compared to air, which makes it the strongest refractive element in the eye. Thus, any corneal alterations or irregularities, as seen in keratoconus, cause major vision impairment [1,2]. Typical signs of KTC range from progressive nearsightedness, irregular astigmatism, distorted or blurred vision, difficulties with night driving, and light sensitivity [3,4]. The incidence and prevalence of keratoconus vary depending on factors such as gender and ethnicity [3]. Nevertheless, keratoconus epidemiology is still unclear. An analysis that covered the entire Danish population reported an estimated prevalence of 86 keratoconus patients per 100 000 residents [5], while a more recent study suggests that the prevalence is significantly higher than around 1:2000 [6]. The condition usually affects both eyes, albeit not necessarily simultaneously. Although the underlying causes are not well understood, there are indications that the disease is multifactorial in origin, related to genetic predisposition and environmental factors such eye rubbing, certain eye conditions and family history [1–3].

In clinical practice the highly irregular shape of advanced keratoconic cornea is easily identified, while the detection of early stages of the disease remains an important challenge. Therefore, developing an efficient technique to assist practitioners with objectively detecting early keratoconus is of paramount importance, as it allows planning more effective treatment strategies and avoiding further acuity loss.

* Corresponding author.Department of Ophthalmology, Antwerp University Hospital, Wilrijkstraat 10, 2650 Edegem, Belgium
*E-mail address:* isarti.ikram@gmail.com (I. Issarti).

https://doi.org/10.1016/j.compbiomed.2019.04.024
Received 23 January 2019; Received in revised form 11 April 2019; Accepted 20 April 2019
0010-4825/ 

**Table 1**
Description of the study groups.

| | $K_{mean}$ (D) | $K_{max}$ (D) | $Pachy_{min}$ (μm) | *Astig* (D) | *I−S* value |
|---|---|---|---|---|---|
| Control *(312 eyes)* | *43.28 ± 1.29 (39.30, 46.60)* | *45.11 ± 1.56 (40.65, 47.80)* | *547.06 ± 30.88 (496, 615)* | *0.86 ± 0.39 (0.2, 1.9)* | *0.20 ± 0.60 (-1.49, -1.33)* |
| Suspect KTC *(90 eyes)* | *42.89 ± 1.51 (39.60, 46.10)* | *44.03 ± 1.50 (41.23, 47.71)* | *530.50 ± 34.37 (458, 591)* | *0.77 ± 0.48 (0.1-2.2)* | *0.64 ± 0.47 (-0.27, -1.61)* |
| Mild KTC *(220 eyes)* | *43.89 ± 2.21 (39.10, 60.80)* | *51.77 ± 3.70 (43.40, 67.90)* | *477.60 ± 34.94 (411, 565)* | *2.98 ± 1.58 (0.10, 7.60)* | *4.74 ± 1.56 (0.7, 8.3)* |
| Moderate KTC *(229 eyes)* | *45.32 ± 3.68 (39.80, 63.60)* | *58.68 ± 6.03 (49.60, 81.40)* | *449.26 ± 39.28 (306, 528)* | *4.01 ± 2.12 (0.2, 12.6)* | *9.50 ± 2.97 (1.67, 19.62)* |

Mean ± SD (range).
I−S, inferior-superior value; KTC, keratoconus; $K_{max}$, maximum keratometry; $Pachy_{min}$, minimum pachymetry; Astig, anterior corneal astigmatism.

Keratoconus diagnosis was initially addressed by the introduction of videokeratography and later by Scheimpflug tomography. Videokeratography provides accurate information about anterior corneal surface shape, while the Scheimpflug tomographer adds information on the posterior corneal surface and corneal thickness. The availability of these measurements led to the introduction of various indices for keratoconus detection. Several authors developed keratoconus detection approaches based on a combination of parameters, such as, keratoconus index (KCI%) [7], inferior superior value (I−S value) [8], keratoconus severity index (KSI) [9], KISA% index [10], keratoconus severity score (KSS) [11], Score [12], Belin/Ambrosio Enhanced Ectasia Display (BAD-D) [13], topographical keratoconus classification (TKC), and more recently Pentacam Random Forest Index (PRFI) [13–33]. Most of these approaches introduce a specific combination of parameters to machine learning algorithms.

Machine learning (ML) algorithms are rapidly gaining importance in the health sector. They are often used to assist in medical diagnosis tasks by capturing the most relevant clinical features of complex data, providing early interpretable results, and helping to choose suitable treatment strategies [34–37]. In the past two decades, several methods have been proposed to automatically detect keratoconus using mathematical models and machine learning [3,22,23,38–44]. These efforts were limited as they only considered 'classic' forms, rather than hybrid approaches of modelling and machine learning. Studies that focused on keratoconus detection employed traditional machine learning to corneal elevation or other extracted clinical parameters, thus neglecting practical restrictions, such as the high variability and sometimes the unstructured nature of corneal tomography data, which requires long computational time. Moreover, the classic algorithms are sensitive to the initial condition and show low accuracies in the earliest cases of the condition. The instability within the earliest cases reduce the performance and the practical use of ML algorithms. However, more stable results are usually achieved in the absence of highly correlated groups, such as advanced keratoconus versus normal or after applying appropriate data preprocessing techniques [45,46]. Some previous works therefore suggested the use of mathematical modelling followed by statistical analysis of clinically derived parameters [28,29,47,48]. These studies are potentially low cost, but mostly platform dependent as they often use proprietary parameters associated with one particular commercial device or manufacturer, thus hampering cross-platform reproducibility of the results.

This paper proposes a computer aided diagnosis (CAD) system for the automatic detection of keratoconus, based on corneal tomography maps and minimum corneal thickness that can be captured by any Scheimpflug device. This system takes the highly unstructured and uninterpretable number of datasets into consideration, as well as the algorithm's instability to the earliest cases of the disease, while also improving the accuracy. The system consists of three main steps. First, a custom-made mathematical model of keratoconic cornea is presented to transform the unstructured topographies to a limited number of meaningful features. Next, a feedforward neural network (FFN) is used to process the model derived features. This type of neural network was selected since it performs better when dealing with corneal topographies [38]. To preserve the stability and improve the accuracies in detecting KTC, a Grossberg architecture was used based on an iterative numerical method, combined with both the feedforward neural network and the mathematical model.

The proposed system overcomes the inherent complexity of tomographical data and permits an accurate detection of keratoconus at the early stage. This framework also optimizes the memory space required in comparison to the direct use of feedforward neural network [38]. Moreover, the CAD has the potential to be platform independent and reproducible on other systems since it only relies on corneal tomography and pachymetry, which is available in all Scheimpflug systems. This requires further validation, however. Finally, the principles of proposed iterative method can be applied to improve the stability and the repeatability of other machine learning techniques.

## 2. Materials and methods

### 2.1. Patient data

This work uses a previously collected database containing the Pentacam (Oculus GmbH, Wetzlar, Germany) Scheimpflug measurements of *851* subjects (aged *33.9 ± 9.5 years*). Of these subjects *312* presented bilateral normal topography, with no systemic or ocular disease, without any prior ocular surgery, and no slit lamp findings suggestive of cornea ectasia. These normal subjects were recruited during a previous epidemiology study [49]. Next, there were *539* keratoconic subjects divided into three groups. The first group contains mild keratoconus (*220* eyes), defined as having a clear cornea, tomography maps compatible with keratoconus (for parameter ranges see Table 1), a Fleischer ring at the apex base, slight thinning, and anterior and/or posterior corneal steepening. Next, there is the moderate keratoconus group, which included *229* subjects that had corneas with slit-lamp findings compatible with keratoconus (see parameters in Table 1), corneal thinning at the apex, Vogt striae, a clearly visible Fleischer ring and corneal tomography compatible with keratoconus. Finally, there was a keratoconus suspect group (*90* eyes), defined as unilateral keratoconus, with one eye presenting a non-symptomatic cornea with normal tomography and no biomicroscopic signs, while the other cornea of the other eye has clinically diagnosed ectasia [24,50]. For each group only, right eyes were considered. A description of the groups is given in the following (Table 1).

All measurements were screened by both an ophthalmologist and an optometrist for quality and validity. Subjects with a self-reported history of ocular surgery, systemic or ocular disease were excluded. The data required for analysis consists of the anterior, posterior corneal elevation for a range of ± 7 mm around the corneal apex in *0.1* mm steps and minimum corneal thickness. The data were created by exporting elevation maps to Pentacam CSV files, which were imported in Matlab (R2017a) in the form of *141* x *141* anterior and posterior matrices, $Z_A(x,y)$ and $Z_P(x,y)$ respectively. The study was approved by the Antwerp University Hospital (UZA, Belgium) Ethical Committee and adhered to the tenets of Declaration of Helsinki. All healthy subjects provided written informed consent before inclusion. Meanwhile, the keratoconic subjects were included retrospectively and required no informed consent according to Belgian law.

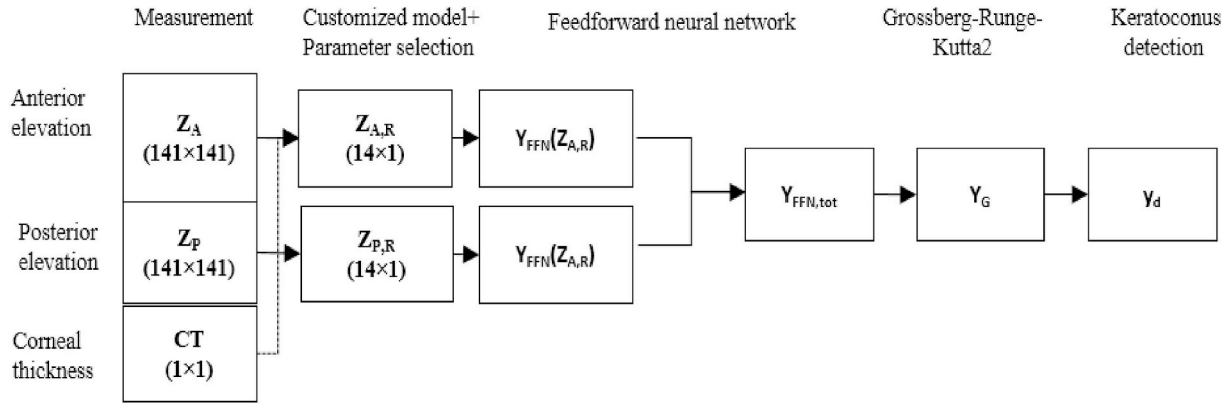


**Fig. 1.** Overview of the modelling and data processing used in the CAD system.

### 2.2. Mathematical model

The proposed framework starts from a customized mathematical model (CMM) to reduce the complexity and dimensionality of the topographical data by transforming each non-meaningful, unstructured matrix $Z_A$ and $Z_P$ to an interpretable vector. This reduces execution time and memory requirements, while improving the performance of the machine learning algorithm. Several mathematical models of the cornea [39,40,49,51–56] can be used to transform and reduce the matrices $Z_A$ and $Z_P$. Previously, Navarro et al. introduced a mathematical decomposition of anterior normal corneal surface by combining a quadric function plus an irregular component [53]. Following the same idea Martínez-Finkelshtein et al. developed an iterative algorithm that dynamically adds terms to a sphere basis function [54], thus enabling a proper modelling of corneal irregularities. By following the same approach, and given the general shape of keratoconic cornea, we opted to use a sum of an ellipsoid surface as a basis function plus a 2-D Gaussian function:

$$z(x, y) = f_s(x, y) + f_G(x, y) \tag{1}$$

where, $z$ is the elevation, $f_G$ the Gaussian function and $f_s$ the ellipsoid function. The z-axis corresponds with the ellipsoid's optical axis, while $z(x,y)$ corresponds with the distance to a reference plan $z = 0$.

The ellipsoid function is given by:

$$f_S(x, y) = C_x.(x - x_0)^2 + C_y.(y - y_0)^2 - cst \tag{2}$$

with $(C_xC_y)$ the curvature of the ellipsoid, $(x_0y_0)$ the ellipsoid center, and $cst$ a constant. Meanwhile, the Gaussian function is given by:

$$f_G = A \cdot exp\left[-\frac{x_{rot}^2}{2\sigma_x^2} - \frac{y_{rot}^2}{2\sigma_y^2}\right] \tag{3}$$

where $A$ is the Gaussian amplitude and $(\sigma_x, \sigma_y)$ the standard deviations. This function uses rotated coordinates $(x_{rot}, y_{rot})$ to allow for keratoconus orientations other than the $x$- or $y$-directions and are given by:

$$\begin{cases} x_{rot} = (x - \mu_x)\cdot cos\theta - (y - \mu_y)\cdot sin\theta \\ y_{rot} = (x - \mu_x)\cdot sin\theta - (y - \mu_y)\cdot cos\theta \end{cases} \tag{4}$$

with $\theta$ the rotation angle and $(\mu_x, \mu_y)$ is the Gaussian center. This model assumes that a normal cornea can be represented by a sum of an ellipsoid with a Gaussian term centered around the minimum corneal thickness, to account for the local irregularities found around the thinnest point of a keratoconic cornea. It is therefore expected that the Gaussian component will behave differently in normal corneas than in keratoconic cases (e.g. centered at the corneal apex and very wide for normal corneas, vs. narrow and inferiorly decentered for keratoconus).

By independently fitting the anterior and posterior corneal elevation $Z_A$ and $Z_P$ to equation (1) the model can be customized to each of the *312* normal and *539* keratoconic subjects. From these fits a set of *17* candidate features was derived to identify keratoconus, which could be divided into three groups: ellipsoid parameters ($C_x$, $C_y$, $x_0$, $y_0$, $cst$), Gaussian parameters ($A$, $\sigma_x$, $\sigma_y$, $\mu_x$, $\mu_y$, $\theta$), and geometric features; ellipsoid volume $S_V$, ellipsoid surface $S_S$, Gaussian volume $G_V$, Gaussian surface $G_S$, Euclidian norm distance between the centers of the anterior and posterior ellipsoid fits, Euclidian norm distance between the centers of the Gaussian and ellipsoid fits. Finally, the minimal corneal thickness (CT), as well as its coordinates $(x_{min}, y_{min})$ were added to the analysis, which are known to correlate well with keratoconus [1,2].

These *17* anterior and 17 posterior candidates features in addition to CT and its coordinates were subsequently analyzed for their suitability to discriminate between normal and keratoconic corneas using Neighborhood Component Analysis for Features Selection (NCAFS), which is one the most efficient techniques for dimensionality reduction [57,58]. The test showed that most parameters perform well in keratoconus detection, except for $C_x$, $C_y$, $\theta$, $G_V$, $cst$, and $x_{min}$. Consequently, $Z_A$ and $Z_P$ were reduced to a set of *14* anterior and *14* posterior parameters ($Z_{A,R}$ and $Z_{P,R}$) that may be used to identify keratoconus (Fig. 1). All the analysis was performed in Matlab.

### 2.3. Computer aided diagnosis

#### 2.3.1. Standard feedforward network applied to tomography data

Feedforward neural network (FFN) is a type of artificial neural network, inspired by biological neurons, that can self-adapt, self-organize and learn from examples, much like their biological counterparts. It is a supervised algorithm that adjusts an input signal $\boldsymbol{X}$ to the desired output $\boldsymbol{Y_d}$ according to an optimization learning rule [59]. The algorithm involves a forward-propagating step followed by a backward-propagating step and it is typically composed of three layers: an input layer that receives $\boldsymbol{m}$ input signals, a hidden layer of $\boldsymbol{n}$ processing units (neurons) with sigmoid activation function $\Gamma_1$, and an output layer with linear activation function $\Gamma_2$. Several optimization algorithms can be used to train the neural network, of which backpropagation and Levenberg-Marquardt are popular choices. In this work, the FFN was configured in Matlab. based on a single hidden layer with *15* neurons, a Logsigmoid activation function, a Levenberg-Marquardt training algorithm, and a learning rate of *0.001*:With $\Gamma_1(t) = \frac{1}{(1+\exp(-t))}$ and $\Gamma_2(t) = t$.

The reduced vectors $Z_{A,R}$ and $Z_{P,R}$ for each subject were considered as network's input, while the output was *0* for normal and *1* for any stage of keratoconus (suspect, mild, moderate). This classification is performed independently for each stage as normal versus suspect KTC, normal versus mild KTC and normal versus moderate KTC.

The structure of the standard feedforward network employed is illustrated in (Fig. 2). The standard approach, based on analyzing a large amount of unstructured elevation data, often leads to overfitting, instability and long training times (in the order of minutes). Using a

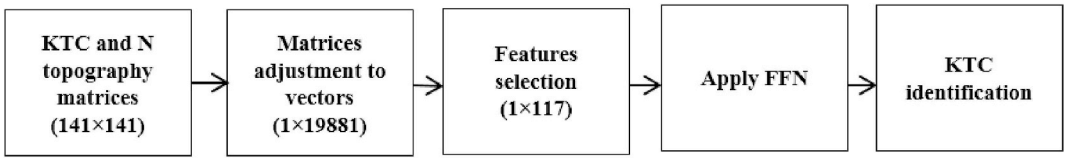


**Fig. 2.** Classical design of the standard FFN applied to topographical data.

mathematical model combined with Grossberg-Runge Kutta architecture may improve the capabilities of FFN, as presented in detail in the next section.

### 2.3.2. Grossberg-Runge Kutta architecture

Grossberg architecture is a competitive type of neural network in which a supervised learning process coordinates the weights of its connections according to a desired output. The convergence of Grossberg algorithm to a single state was already demonstrated in the literature [60]. The learning process is based on a simple explicit rule for weights adjustment between inputs and outputs and may be regarded as a mathematical Cauchy problem (eq. (5)) that admits a unique solution under certain assumptions. Several iterative numerical methods have been suggested to approximate the solution $w_{ij}(t)$ of problems (eq. (5)) [61], often referred to as being either *explicit* or *implicit*. These methods are based on integration and discretization processes that lead to different levels of precision, convergence, stability and computational cost. Runge Kutta is one of the best known of these techniques [62–64]. In our case, the Cauchy problem is given by:

$$\begin{cases} \frac{dw_{ij}}{dt} = f(t, w_{ij}(t)) \\ w(t=0)\ given \end{cases} \quad (5)$$

Where $w_{ij}$ is the weight matrix of the Grossberg network and $f$ is the training rule.

Here, the explicit second order Runge Kutta (RK2) was suggested as a learning rule of the Grossberg layer, which is supposed to lead to better convergence and stability compared to the traditionally used learning process. This explicit rule of Grossberg architecture based RK2 is:

$$\begin{cases} v_{ij}(t+\Delta t) = w_{ij}(t) + \delta.\,(y_i - v_{ij}(t)).\,z_i \\ w_{ij}(t+\Delta t) = w_{ij}(t) + \frac{\Delta t}{2}.\,[\delta.\,(y_i - w_{ij}(t)).\,z_i + \delta.\,(y_i - v_{ij}(t+1)).\,z_i] \\ w_0\ initial\ condition \end{cases} \quad (6)$$

Where, $v_{ij}$ is an intermediate neuronal connection, $z_i$ is the feedforward network output, $\Delta t$ is a time step, $\delta$ is the learning rate of Grossberg network, $w_0$ is the initial weight. The Grossberg-RK2 was implemented in Matlab with $\delta < 1$ and $\Delta t = 1$, the initial weights were generated randomly between [0,1].

### 2.3.3. Hybrid machine learning algorithm (CMM-FFN)

The hybrid machine learning algorithm was implemented by combining the custom mathematical model with an adapted FFN according to a probabilistic function (eq. (7)). In practice the FFN with the previous standard configurations (section 2.3.1) were trained on the reduced anterior data $Z_{A,R}$ and the reduced posterior data $Z_{P,R}$, separately, yielding responses $y_{Ante}$ and $y_{Post}$. These responses were then inserted into the probability function (eq. (7)) to give more weight to the posterior layer, considering that keratoconus often appears on the posterior surface first [65]. This yields a total response function $y_{FFN,tot}$ (Fig. 1), defined as follows:

$$Y_{FFN,tot} = p_1 \cdot y_{Ante}(Z_{A,R}) + p_2 \cdot y_{Post}(Z_{P,R}) \text{ with } p_2 > p_1 \quad (7)$$

During the entire training process all weights are optimized to ensure that the algorithm response $y_{FFN,tot}$ agrees with the original training data $y_d$ as much as possible. Beforehand, weight parameters $p_1$ and $p_2$ are estimated according to the previous domination of the posterior surface to approach the desired response as follow:

$$\underset{p_1<p_2\in[0,1]}{Maxf}(p_1, p_2) = p_1 \cdot y_{Ante} + p_2 \cdot y_{Post} \quad (8)$$

The computer aided diagnosis system was obtained by combining the CMM-FFN with Grossberg network, therefore, the final output $y_{FFN,tot}$ is given to the Grossberg layer to correct the weights and improve the identification process.

The computer aided design algorithm is then summarized. by the following steps:

1) Fit $Z_A$ (x,y) and $Z_P$(x,y) to the custom mathematical model CMM equation (1).
2) Derive and reduce CMM features to $Z_{A,R}$ and $Z_{P,R}$.
3) Train FFN-based on [Inputs, Outputs] = [ $Z_{A,R}$, $y_d$] and compute the algorithm's output $y_{Anter}$(Anterior).
4) Train FFN-based on [Inputs, Outputs] = [ $Z_{P,R}$, $y_d$] and compute the algorithm's output $y_{Post}$(Posterior).
5) Estimate $p_1$, $p_2$ according to: $\underset{p_1<p_2\in[0,1]}{Maxf}(p_1, p_2) = p_1 \cdot y_{Ante} + p_2 \cdot y_{Post}$
6) Compute the final output according to: $Y_{FFN,tot} = p_1 \cdot y_{Ante}(Z_{A,R}) + p_2 \cdot y_{Post}(Z_{P,R})$
7) Implement the Grossberg Layer for the input output data [ $Y_{FFN,tot}$, $Y_d$]
8) Adjust the weights of the Grossberg Layer based on RK2 numerical schemes equation (6).
9) Compute the finale output $Y_G = < W, Y_{FFN,tot} >$

### 2.3.4. Validation

To evaluate the performance of the proposed CAD for keratoconus detection, 10-fold cross validation technique was used. This uses data more efficiently than traditional holdout validation. The latter randomly splits the dataset into training sets (*70%*) and validates the classifier with the other *30%*. 10-fold cross validation splits the datasets into *10* independent groups, *9* of which are used for training, while the last group is used for validation. This process is performed a total of *10* times, until each group has been used independently as a test set. This technique better indicates classifier performance, while using new data and providing a more accurate estimation of the error rate [66]. For each of the *10* repetitions the accuracy, precision, sensitivity, and specificity were computed, as defined in (Table 2) [67]. However, to evaluate the general performance of CAD versus CMM-FFN, holdout validation and confusion matrix were used based on the same validation criteria defined in (Table 2).

The final accuracy, sensitivity, specificity, and precision values for 10-fold cross validation were computed as the average of the 10 repetitive times. Both validation techniques (10-fold cross validation, holdout validation) were repeated *20* times and gave roughly the same results each time. Finally, Receiver Operating Characteristic (ROC) curves were used to compare the discriminative abilities of the proposed approach versus CMM-FFN, BADD, and TKC.

## 3. Results

### 3.1. Performance of ellipsoid -Gaussian model

The customized model accurately describes the anterior and

**Table 2**
Definition of validation criteria.

| | | |
|---|---|---|
| True positive | TP | Number of KTC cases identified correctly |
| True negative | TN | Number of N cases identified correctly |
| False positive | FN | Number of KTC cases classified as normal |
| False negative | FP | Number of normal classified as KTC |
| Accuracy | (TP + TN)/(TP + FP + FN + TN) | Percentage of dataset classified correctly |
| Sensitivity | TP/(TP + FN) | Percentage of KTC cases correctly classified. |
| Specificity | TN/(TN + FP) | Percentage of normal cases correctly classified. |
| Precision | TP/(TP + FP) | The ratio of the correctly classified KTC, high precision relates to low false positive. |
| Cut-off | | Value or point designed as a limit of a group. |

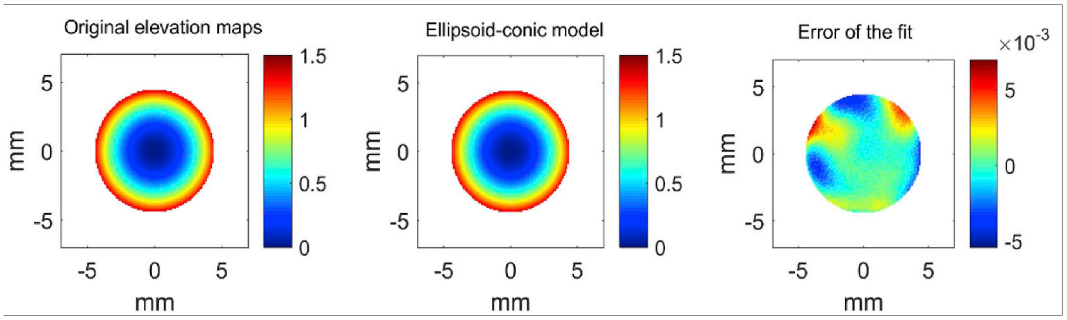


**Fig. 3.** Representative, randomly chosen example of original elevation topography vs. CMM topography, color bars expressed in mm. Also, x and y axis are expressed in mm. (For interpretation of the references to color in this figure legend, the reader is referred to the Web version of this article.)

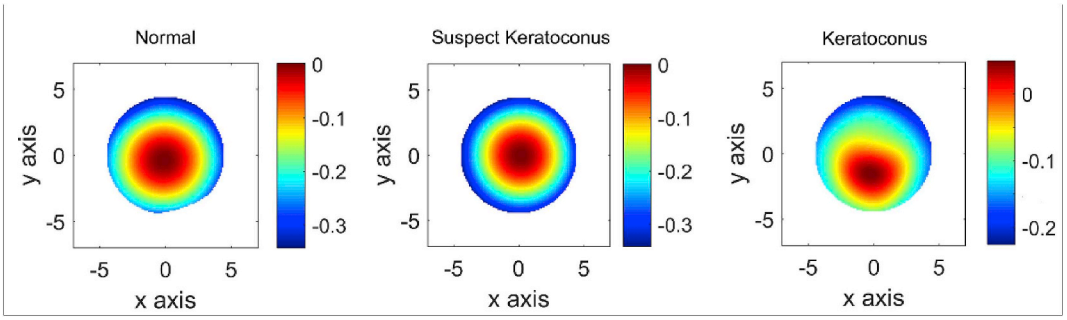


**Fig. 4.** Representative, randomly chosen examples of the Gaussian term in normal, keratoconus suspect, and moderate keratoconus, color bars expressed in mm. Also, x and y axis are expressed in mm. (For interpretation of the references to color in this figure legend, the reader is referred to the Web version of this article.)

posterior surfaces of both keratoconic and normal corneas. In the center ( ± 4 mm from the apex) of anterior surface, the best observed error was $\xi \in O(10^{-3})$ *mm*, while it was $\xi \in O(10^{-2})$ *mm* at the periphery (radius 4 mm–5 mm) The same best error of $\xi \in O(10^{-3})$ *mm* was achieved in the center and the periphery of posterior surface (Fig. 3). The model allows for a clear topographic distinction between clinical keratoconic and normal corneas since the Gaussian of normal corneas forms a small, near-perfect circle with a center very close to the apex in the *x* direction (i.e. $\mu_x \approx 0$) and within ± 2 mm from the apex in the *y* direction (i.e. $\mu_y \varepsilon$ [*–2, 2*]; (Fig. 4)). In most moderate keratoconus cases the Gaussian narrows and undergoes an inferior shift towards $\mu_y \varepsilon$ [*–4, –2*]. In suspect keratoconus the CMM was unable to clearly distinguish between early keratoconus and normal (Fig. 4), demonstrating the need for using the machine learning algorithms.

### 3.2. Performance of the CAD

#### 3.2.1. Influence of sample size

To evaluate the importance of sample size on the results, a balanced set of *312* keratoconus cases, equal to the size of normal group, was randomly selected from the three keratoconus stages (Table 1). Similarly, an imbalanced set of *150* keratoconus was randomly selected from the *312* keratoconus. The validation criteria; accuracy, sensitivity, specificity, precision and confusion matrix were examined for both groups (balanced and imbalanced). The comparison was given for both CAD and CMM-FFN.

The highest accuracy for the classification of normal versus keratoconus during the validation step for the balanced groups was *98.4%* for CAD versus *96.4%* for CMM-FFN (Table 3). Since the size of groups might influence the results, this analysis was repeated by training the algorithm using the imbalanced groups of normal and keratoconus, yielding nearly identical results as before for both CAD and CMM-FNN, and show a lower average of change in the sensitivity of CMM-FFN, however, the accuracy and the sensitivity of CAD were higher than the accuracy and the sensitivity of CMM-FFN (Table 3). The results demonstrate the high performance and the general stability of CAD comparing with CMM-FFN when applied to imbalanced data sets.

The normal cases were nearly all classified correctly, with *9* misclassifications of keratoconus as normal for computer aided diagnosis system (Table 4) against *21* misclassifications for the feedforward neural network with the custom mathematical model (Tables 4 and 5). The obtained results therefore indicate that adding Grossberg-RK2 leads to improve the values of the validation criteria.

#### 3.2.2. Comparison between methods

The proposed computer diagnosis system results in nearly identical

**Table 3**
Performance of CAD vs. CMM-FFN using Holdout Validation.

| | CAD | | | | CMM-FFN | | | |
|---|---|---|---|---|---|---|---|---|
| | Accu-racy | Sensi-tivity | Speci-ficity | Preci-sion | Accu-racy | Sensi-tivity | Speci-ficity | Preci-sion |
| **Imbalanced dataset** | | | | | | | | |
| *Normal (312)* | *98.2%* | *96.0%* | *99.3%* | *98.6%* | *96.3%* | *91.3%* | *99.3%* | *98.5%* |
| *Keratoconus (150)* | | | | | | | | |
| **Balanced Dataset** | | | | | | | | |
| *Normal (312)* | *98.4%* | *97.1%* | *99.6%* | *99.6%* | *96.4%* | *93.2%* | *99.6%* | *99.6%* |
| *Keratoconus (312)* | | | | | | | | |

**Table 4**
Confusion matrix of CMM-FFN.

| Predicted class<br>Actual class | Keratoconus | Normal |
|---|---|---|
| Keratoconus *(N = 312)* | *291* | *21* |
| Normal *(N = 312)* | *1* | *311* |

**Table 5**
Confusion matrix of the CAD.

| Predicted class<br>Actual class | Keratoconus | Normal |
|---|---|---|
| Keratoconus *(N = 312)* | *303* | *9* |
| Normal *(N = 312)* | *1* | *311* |

**Table 6**
Validation of The CAD system.

| | | 10-Fold cross validation | | |
|---|---|---|---|---|
| | | KTC suspect *vs.* Normal | Mild KTC *vs.* Normal | Moderate KTC *vs.* Normal |
| CAD | Accuracy | *96.56%* | *99.40%* | *99.58%* |
| | Sensitivity | *97.78%* | *98.81%* | *99.91%* |
| | Specificity | *95.56%* | *99.71%* | *99.90%* |
| | Precision | *95.65%* | *99.71%* | *99.90%* |
| | Cut-Off | *0.82* | *1* | *1* |
| FFN-CMM | Accuracy | *93.67%* | *99.55%* | *99.72%* |
| | Sensitivity | *90.00%* | *99.55%* | *99.44%* |
| | Specificity | *94.35%* | *99.56%* | *99.90%* |
| | Precision | *94.27%* | *99.56%* | *99.90%* |
| | Cut-Off | *0.82* | *1* | *1* |
| BADD | Accuracy | *89.00%* | *99.90%* | *99.02%* |
| | Sensitivity | *83.00%* | *99.85%* | *99.90%* |
| | Specificity | *95.00%* | *97.48%* | *98.05%* |
| | Precision | *95.00%* | *97.57%* | *98.15%* |
| | Cut-Off | *0.68* | *0.98* | *1* |
| TKC | Accuracy | *79.00%* | *93.11%* | *99.99%* |
| | Sensitivity | *58.00%* | *86.22%* | *99.99%* |
| | Specificity | *99.70%* | *99.99%* | *99.99%* |
| | Precision | *99.62%* | *99.99%* | *99.99%* |
| | Cut-Off | *0* | *1* | *1* |

results for mild and moderate KTC comparing with custom made mathematical model combined with feedforward neural network. However, the CAD is also able to successfully identify the earliest cases of keratoconus that cannot be detected clinically by looking at tomography maps alone, with an accuracy of 96.56% in detecting suspect KTC versus 93.67% for CMM-FFN (Table 6). In addition, the proposed approach outperformed Belin/Ambrosio Deviation (BADD) and Topographical Keratoconus Classification (TKC) systems in terms of accuracy, sensitivity, specificity, and precision for suspect KTC detection, however, CAD shows nearly similar results in detecting mild and moderate stages in comparison with the previously described methods (Table 6). The high performance of CAD is also seen in the comparative ROC curves for the classification of keratoconus versus normal and suspect keratoconus versus normal (Fig. 5). Consequently, the algorithm accurately distinguishes keratoconus corneas from normal corneas at different stages.

### 3.2.3. Computational efficiency

The computational efficiency of the standard FFN, CMM-FFN and CAD is compared based on keratoconus groups (section 3.21) and using Holdout validation technique. The number of iterations, execution time and CPU time were selected from the most representative values, while training at least 20 times. Obtained results showed that the proposed algorithm overcomes the data complexities and reduces the computation time by *70%* (Table 7). The validation performance of FFN-CMM converges after *17* iterations (epochs), considerably faster and with a considerably less variable error than standard FFN (Figs. 6 and 7). The stability and the convergence of FFN-CMM and CAD was investigated and presented in (Fig. 8) and (Table 7). CAD showed better convergence and less error variations, proving the distinct advantage of adding the Grossberg-RK2 layer to the standard algorithm.

The CAD showed an improvement in accuracy compared with the standard feedforward network (Table 7), that reached an accuracy of *98.4%* vs *92.0%* and a sensitivity of *97.1%* vs. *83.7%*.

## 4. Discussion

Many different modelling approaches have been suggested to assist practitioners with differentiating between normal and keratoconic corneas based on mathematical models [41,47,48,53–56] or machine learning algorithms. Other approaches consist of a direct statistical analysis of clinical quantitative parameters, such as corneal tomography, corneal topography or corneal pachymetry [10,28,29,32,33,68–72]. Most previous publications were platform dependent and rely on parameters that are often not provided by other devices, with very few exceptions [11,30,31]. This study presents a computer aided diagnosis system (CAD), based only on the elevation data and minimum corneal thickness, that can be captured by various ophthalmic devices. This might increase the interest and the potential reproducibility of the study. To the best of our knowledge, this is the first elevation-pachymetry based adapted algorithm that does not require additional clinical parameters. Moreover, the proposed approach is the first to consider the instability of machine learning algorithm for the early keratoconus detection.

Many earlier studies were based on classic machine learning algorithms [9,12,12,24,24,25,25,38–40,44,73–78] that did not consider the practical limitations of dealing with large, unstructured datasets and cost. The proposed framework overcomes this by reducing the (*141* × *141*) elevation matrices to *14* structured and meaningful features for each subject (Fig. 1). Consequently, the CAD shows a better classification performance than the standard feedforward network and reduces the computation time by *70%* (Table .7). The CAD system also includes

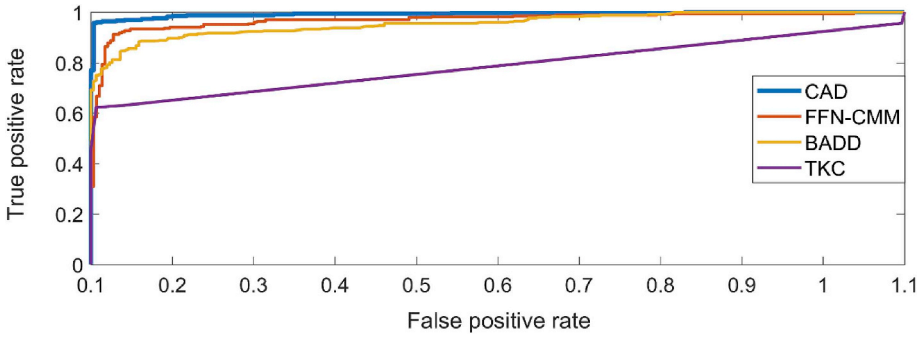


**Fig. 5.** Comparative ROC curves for the suspect KTC vs Normal.

**Table 7**
Comparison of the standard FFN, CMM- FFN, and CAD.

| | FNN | FFN-CMM | CAD |
|---|---|---|---|
| Accuracy | *92.2%* | *96.4%* | *98.4%* |
| Sensitivity | *83.7%* | *93.2%* | *97.1%* |
| Specificity | *99.0%* | *99.0%* | *99.6%* |
| Precision | *98.9%* | *99.6%* | *99.6%* |
| Max. iterations | *5* | *20* | *20* |
| Number of features | *117* | *14* | *14* |
| Execution time | *12.9 s* | *3.1 s* | *4.8 s* |
| CPU time | *248.0 s* | *20.0 s* | *6.1 s* |

an explicit Grossberg layer based Runge Kutta numerical schemes that increase the accuracy and stability of the standard feedforward neural network (Figs. 6–8), allowing the system to preserve the stability at different stages of the disease. Moreover, this work demonstrates that it is possible to improve keratoconus detection without using a large set of interdependent clinical parameters, and that the same approach can be used for detecting earlier stages of the condition (Table 6). The influence of the imbalanced data sets was investigated and validated using hold out validation technique (Tables 3–5), which demonstrated that the CAD is more stable and, more accurate results were reached by adding the Grossberg architecture.

A comparative study between the CAD and other available approaches for keratoconus detection at different stages was considered and validated using the 10-fold cross validation technique and ROC curves. This indicated that the CAD is indeed highly accurate in distinguishing clinical keratoconus from normal eyes with an accuracy of *99.58%* (sensitivity: 99.91%; specificity: *99.90%*; precision: *99.90%*) for moderate cases and *99.40%* (sensitivity: *98.81%;* specificity: *99.71%*; precision: *99.71%*) for mild keratoconus. For these cases, the CAD provided nearly similar results as the feedforward combined with mathematical model (CMM-FFN), Belin/Ambrosio Deviation (BADD), and Topographical Keratoconus Classification (TKC) (Table 6). For the classification of keratoconus suspect, however, it improved on the performance of the other systems with an accuracy of *96.56%* (sensitivity: *97.78%;* specificity: *95.56%*; precision: *95.65%*), compared to an accuracy of *93.67%* for CMM-FFN (sensitivity: *90.00%;* specificity: *94.35%*; precision: *94.27%*), *89.00%* for BADD (sensitivity: *83.00%;* specificity: *95.00%*; precision: *95.00%*), and an accuracy of *79.00%* for TKC (sensitivity: *58.00%;* specificity: *99.70%*; precision: *99.62%*). CAD can therefore accurately detects suspect keratoconus by dealing with the ambiguities found in the earliest cases of the disease and improving the convergence (Fig. 8).

In addition, the CPU time of the CAD was *6.1 s* vs. *20.0 s* using CMM-FFN and *248.0 s* using only FFN, which demonstrate the computational efficiency of the proposed approach versus the traditional machine learning algorithms. Moreover, the achieved results showed the importance of custom-made mathematical model in reducing computational time and that the Grossberg-RK2 preserves the stability without causing an increase in computational cost.

Earlier work on detecting advanced KTC using Zernike polynomial fitting and decision trees reported an accuracy of *92.0%* and an area under the ROC curve of *97.0%* [39]. A follow-up study examined two orthogonal polynomials for spatial data transformation in conjunction with decision tree yielded to an easily interpretable results and less accuracy [40]. Sousa et al. [38] evaluated three machine learning classifiers for keratoconus detection, reporting a sensitivity of 99.0% with both support vector machine and multilayer perceptron against *98.0%* with radial basis functions [38]. Another attempt to detect advanced keratoconus used discriminant functions to analyze corneal asymmetry parameters reaching a sensitivity of *94.0%* and specificity of *100%* [75]. More recent work analyzed tomographic, topographic and pachymetry data using support vector machine results an accuracy of *98.2%* (sensitivity: *95.0%*; specificity: *99.3%*; precision: *97.9%*) for keratoconus versus normal and an accuracy of *97.3%* (sensitivity: *92.0%*; specificity: *97.7%*; precision: *78.8%*) for early keratoconus [74]. While the latter study achieved very good results for keratoconus detection, their early keratoconus group includes keratoconus ectasia characteristics and the approach was based on a large number of datasets. The same limitation of ectatic characteristics was also encountered in another study [73] that used decision trees applied directly to *55* topographical parameters, and reported a sensitivity of

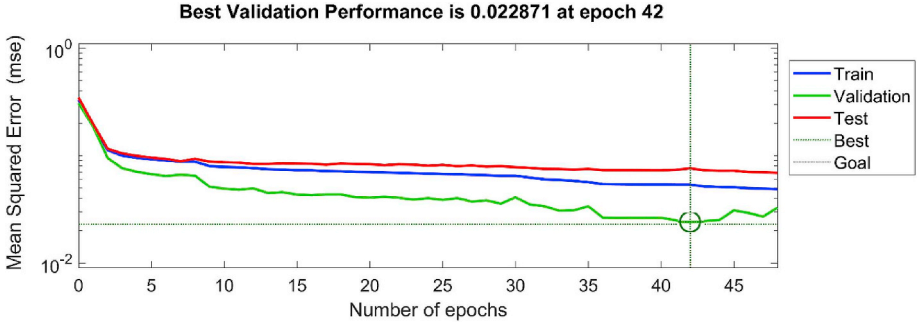


**Fig. 6.** Validation performance of the standard FFN.

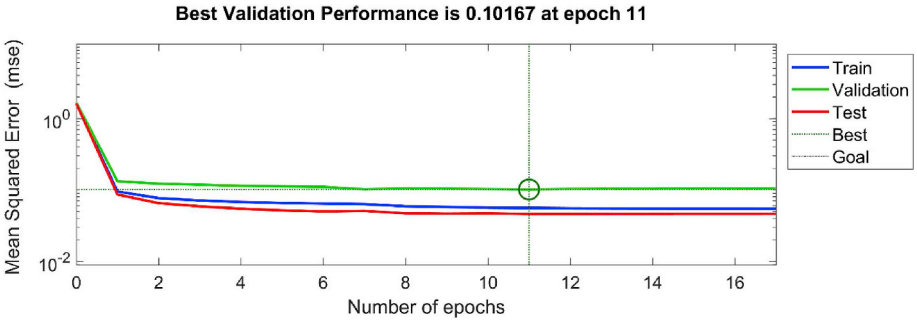


**Fig. 7.** Validation performance of the CMM-FFN.

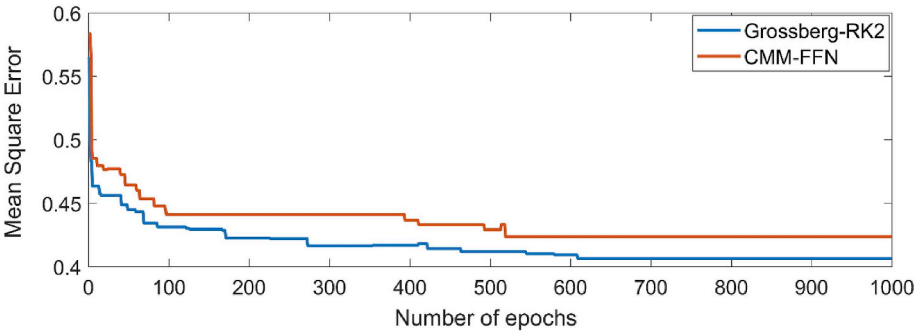


**Fig. 8.** Error changes with respect to the level of variations.

*93.6%* and specificity of *97.2%* for distinguishing early from normal, and a sensitivity of *100%* and specificity of *99.5%* for advanced keratoconus. Meanwhile, other studies achieved a better sensitivity for earlier cases [73,74]. Similarly, our previous study using Support Vector Machine applied to a set of *22* Tomographical parameters from the Pentacam [22,23] reported an accuracy of *93.1%*, sensitivity of *79.1%* and specificity of *97.9%* when classifying early KTC, and accuracy of *98.9%*, sensitivity of *99.1%* and specificity of *98.5%* for advanced cases. Finally, Lopes et al. [77] examined tomographical data with various machine learning techniques, and achieved best results using random forests, reporting a sensitivity of *85.2%* and specificity of *96.6%* for suspect keratoconus. A more complete summary of studies that discriminate between normal and keratoconus was given in our previous study [23], and several reviews [79,80].

The proposed algorithm (CAD) is therefore comparable or higher to the earlier approaches for keratoconus detection. This is important since, even though recent studies report good results on earlier approaches, one often sees that their methodologies are based on proprietary parameters associated with one specific ophthalmological device. By modelling tomography data, which could be acquired from any commercially available Scheimpflug topographer, we overcame this issue while increasing the potential reproducibility of our study. Moreover, it deals with the problem of data complexity and the long training time (in the order of minutes or even hours for classical machine learning), while enhancing the detection accuracy for all stages of the disease. The proposed CAD deals with an important practical issue related to the instability of the algorithm while detecting ambiguous cases such as keratoconus suspect.

There are some limitations to this study that need to be acknowledged, most notably some false positive misclassifications that may be related to the clinical similarities between healthy and suspect stages of the disease (Tables 4–5). This issue can potentially be improved by adding other platform independent parameters. Another major limitation is related to the clinical definition of keratoconus suspect. Some authors define this group as corneas that show skewed radial axes as a first sign of KTC [76–78], while others considered it as the non-diseased cornea, while the fellow cornea is diagnosed with keratoconus [22,24,50,81,82]. This work uses the latter definition since it is the most rigorous in the literature. However, using this strict definition comes at the price that some healthy corneas may be incorrectly considered as keratoconus suspect. This hinders direct comparisons with previous studies that used another definition, as it would lead to differences in accuracies, specificities, and sensitivities. Finally, the platform independence and the reproducibility of the proposed approach still need to be validated.

Further research could address additional issues, such as validating the CAD system using additional data collected at independent medical centers and using other devices. Another aspect to be explored is the ability of the algorithm to provide a scoring system for keratoconus progression, which forms another open and challenging question.

In conclusion, this study presented a computer aided diagnosis system that can accurately detect keratoconus at different stages. In principle this method should be platform independent, but this remains to be confirmed. Furthermore, the algorithm overcomes the data complexities issues, reduces the computation time and preserves the stability. The proposed framework presents an easy platform that can be used to assist ophthalmologist with the process of decision making. Finally, the main principles of the proposed strategy can be adapted to detect other diseases and yet reduces computation time.

## Declaration of interests

None.

## Details of funding

This work was supported in part by a research grant by the Flemish government agency for Innovation by Science and Technology (grant no. TBM-T000416N).

## References

[1] D.P. Piñero, J.C. Nieto, A. Lopez-Miguel, Characterization of corneal structure in keratoconus, J. Cataract Refract. Surg. 38 (2012) 2167–2183, https://doi.org/10.

1016/j.jcrs.2012.10.022.
[2] Y.S. Rabinowitz, Keratoconus. Surv Ophthalmol 42 (1998) 297–319.
[3] V. Mas Tur, C. MacGregor, R. Jayaswal, D. O'Brart, N. Maycock, A review of keratoconus: diagnosis, pathophysiology, and genetics, Surv. Ophthalmol. 62 (2017) 770–783, https://doi.org/10.1016/j.survophthal.2017.06.009.
[4] M. Romero-Jiménez, J. Santodomingo-Rubido, J.S. Wolffsohn, Keratoconus: a review, Contact Lens Anterior Eye 33 (2010) 157–166, https://doi.org/10.1016/j.clae.2010.04.006.
[5] K. Nielsen, J. Hjortdal, E. Aagaard Nohr, N. Ehlers, Incidence and prevalence of keratoconus in Denmark, Acta Ophthalmol. Scand. 85 (2007) 890–892, https://doi.org/10.1111/j.1600-0420.2007.00981.x.
[6] N. Hafezi, F. Hafezi, Is keratoconus really rare? Keratoconus Really Rare 10 (2) (2017) 91–92, https://doi.org/10.17925/USOR.2017.10.02.91.
[7] N. Maeda, S.D. Klyce, M.K. Smolek, H.W. Thompson, Automated keratoconus screening with corneal topography analysis, Investig. Ophthalmol. Vis. Sci. 35 (1994) 2749–2757.
[8] Y.S. Rabinowitz, Videokeratographic indices to aid in screening for keratoconus, J Refract Surg Thorofare NJ 11 (1995) 371–379.
[9] M.K. Smolek, S.D. Klyce, Current keratoconus detection methods compared with a neural network approach, Investig. Ophthalmol. Vis. Sci. 38 (1997) 2290–2299.
[10] Y.S. Rabinowitz, K. Rasheed, KISA% index: a quantitative videokeratography algorithm embodying minimal topographic criteria for diagnosing keratoconus, J. Cataract Refract. Surg. 25 (1999) 1327–1335.
[11] T.T. McMahon, L. Szczotka-Flynn, J.T. Barr, R.J. Anderson, M.E. Slaughter, J.H. Lass, et al., A new method for grading the severity of keratoconus: the Keratoconus Severity Score (KSS), Cornea 25 (2006) 794–800, https://doi.org/10.1097/01.ico.0000226359.26678.d1.
[12] CASSETTE NB Studio, A. Saad, D. Gatinel, Validation of a new scoring system for the detection of early forme of keratoconus, Int. J. Keratoconus Ectatic Corneal Dis. 1 (2) (2012) 100–108 Docteur Damien Gatinel n.d. https://www.gatinel.com/2012/09/saad-a-gatinel-d-validation-of-a-new-scoring-system-for-the-detection-of-early-forme-of-keratoconus-int-j-kerat-ect-cor-dis-2012-12100-108/ , Accessed date: 29 November 2018.
[13] M.W. Belin, S.S. Khachikian, Keratoconus/Ectasia Detection with the Oculus Pentacam : Belin/Ambrósio Enhanced Ectasia Display, (2008).
[14] D. Muckenhirn, Die Anpassung von asphärischen Kontaktlinsen bei Keratokonus unter Berücksichtigung der geometrisch-optischen Verhältnisse der Hornhaut, Neues Opt J 5 (1984) 87–94.
[15] J.H. Krumeich, J. Daniel, A. Knülle, Live-epikeratophakia for keratoconus, J. Cataract Refract. Surg. 24 (1998) 456–463, https://doi.org/10.1016/S0886-3350(98)80284-8.
[16] J.L. Alió, M.H. Shabayek, Corneal higher order aberrations: a method to grade keratoconus, J. Refract. Surg. 22 (2006) 539–545, https://doi.org/10.3928/1081-597X-20060601-05.
[17] X. Li, H. Yang, Y.S. Rabinowitz, Keratoconus: classification scheme based on videokeratography and clinical signs, J. Cataract Refract. Surg. 35 (2009) 1597–1603, https://doi.org/10.1016/j.jcrs.2009.03.050.
[18] M.W. Belin, J.K. Duncan, Keratoconus: the ABCD grading system, Klin. Monatsbl. Augenheilkd. 233 (2016) 701–707, https://doi.org/10.1055/s-0042-100626.
[19] N. Gupta, B.L. Trindade, J. Hooshmand, E. Chan, Variation in the best fit sphere radius of curvature as a test to detect keratoconus progression on a scheimpflug-based corneal tomographer, J Refract Surg Thorofare NJ 34 (2018) 260–263, https://doi.org/10.3928/1081597X-20180206-03 1995.
[20] Y.S. Rabinowitz, P.J. McDonnell, Computer-assisted corneal topography in keratoconus, J. Refract. Surg. 5 (1989) 400–408, https://doi.org/10.3928/1081-597X-19891101-10.
[21] R. Ishii, K. Kamiya, A. Igarashi, K. Shimizu, Y. Utsumi, T. Kumanomido, Correlation of corneal elevation with severity of keratoconus by means of anterior and posterior topographic analysis, Cornea 31 (2012) 253–258, https://doi.org/10.1097/ICO.0B013E31823D1EE0.
[22] I. Ruiz Hidalgo, P. Rodriguez, J.J. Rozema, S. Ní Dhubhghaill, N. Zakaria, M.-J. Tassignon, et al., Evaluation of a machine-learning classifier for keratoconus detection based on Scheimpflug tomography, Cornea 35 (2016) 827, https://doi.org/10.1097/ICO.0000000000000834.
[23] I. Ruiz Hidalgo, J.J. Rozema, A. Saad, D. Gatinel, P. Rodriguez, N. Zakaria, et al., Validation of an objective keratoconus detection system implemented in a Scheimpflug tomographer and comparison with other methods, Cornea 36 (2017) 689, https://doi.org/10.1097/ICO.0000000000001194.
[24] A. Saad, D. Gatinel, Topographic and tomographic properties of forme fruste keratoconus corneas, Investig. Ophthalmol. Vis. Sci. 51 (2010) 5546–5555, https://doi.org/10.1167/iovs.10-5369.
[25] B.T. Lopes, I.C. Ramos, M.Q. Salomão, F.P. Guerra, S.C. Schallhorn, J.M. Schallhorn, et al., Enhanced tomographic assessment to detect corneal ectasia based on artificial intelligence, Am. J. Ophthalmol. 195 (2018) 223–232, https://doi.org/10.1016/j.ajo.2018.08.005.
[26] I. Issarti, A. Consejo, J.J. Rozema, Elevation-based detection of keratoconus, Investig. Ophthalmol. Vis. Sci. 59 (2018) 5810–5810.
[27] I. Issarti, J. Rozema, A. Consejo, Corneal modeling and Keratoconus identification, Biomath Commun Suppl 5 (2018).
[28] S.A. Read, M.J. Collins, D.R. Iskander, B.A. Davis, Corneal topography with Scheimpflug imaging and videokeratography: comparative study of normal eyes, J. Cataract Refract. Surg. 35 (2009) 1072–1081, https://doi.org/10.1016/j.jcrs.2009.01.020.
[29] P. Kosekahya, M. Caglayan, M. Koc, H. Kiziltoprak, K. Tekin, C.U. Atilgan, Longitudinal evaluation of the progression of keratoconus using a novel progression display, Eye Contact Lens (2019), https://doi.org/10.1097/ICL.0000000000000582.
[30] D. Ramos-López, A. Martínez-Finkelshtein, G.M. Castro-Luna, D. Piñero, J.L. Alió, Placido-based indices of corneal irregularity, Optom Vis Sci Off Publ Am Acad Optom 88 (2011) 1220–1231, https://doi.org/10.1097/OPX.0b013e3182279ff8.
[31] D. Ramos-López, A. Martínez-Finkelshtein, G.M. Castro-Luna, N. Burguera-Gimenez, A. Vega-Estrada, D. Piñero, et al., Screening subclinical keratoconus with placido-based corneal indices, Optom Vis Sci Off Publ Am Acad Optom 90 (2013) 335–343, https://doi.org/10.1097/OPX.0b013e3182843f2a.
[32] O. Golan, A.L. Piccinini, E.S. Hwang, I.M. De Oca Gonzalez, M. Krauthammer, S.S. Khandelwal, et al., Distinguishing highly asymmetric keratoconus eyes using dual scheimpflug/placido analysis, Am. J. Ophthalmol. (2019), https://doi.org/10.1016/j.ajo.2019.01.023.
[33] H. Hashemi, A. Beiranvand, A. Yekta, A. Maleki, N. Yazdani, M. Khabazkhoob, Pentacam top indices for diagnosing subclinical and definite keratoconus, J Curr Ophthalmol 28 (2016) 21–26, https://doi.org/10.1016/j.joco.2016.01.009.
[34] R.C. Deo, Machine learning in medicine, Circulation 132 (2015) 1920–1930, https://doi.org/10.1161/CIRCULATIONAHA.115.001593.
[35] N. Peek, C. Combi, R. Marin, R. Bellazzi, Thirty years of artificial intelligence in medicine (AIME) conferences: a review of research themes, Artif. Intell. Med. 65 (2015) 61–73, https://doi.org/10.1016/j.artmed.2015.07.003.
[36] G. Dorffner, G. Porenta, On using feedforward neural networks for clinical diagnostic tasks, Artif. Intell. Med. 6 (1994) 417–435, https://doi.org/10.1016/0933-3657(94)90005-1.
[37] J.C. Augusto, Temporal reasoning for decision support in medicine, Artif. Intell. Med. 33 (2005) 1–24, https://doi.org/10.1016/j.artmed.2004.07.006.
[38] M.B. Souza, F.W. Medeiros, D.B. Souza, R. Garcia, M.R. Alves, Evaluation of machine learning classifiers in keratoconus detection from orbscan II examinations, Clinics 65 (2010) 1223–1228.
[39] M.D. Twa, S. Parthasarathy, C. Roberts, A.M. Mahmoud, T.W. Raasch, M.A. Bullimore, Automated decision tree classification of corneal shape, Optom Vis Sci Off Publ Am Acad Optom 82 (2005) 1038–1046.
[40] K. Marsolo, M. Twa, M.A. Bullimore, S. Parthasarathy, Spatial modeling and classification of corneal shape, IEEE Trans. Inf. Technol. Biomed. 11 (2007) 203–212, https://doi.org/10.1109/TITB.2006.879591.
[41] C.J. Roberts, W.J. Dupps, Biomechanics of corneal ectasia and biomechanical treatments, J. Cataract Refract. Surg. 40 (2014) 991–998, https://doi.org/10.1016/j.jcrs.2014.04.013.
[42] I. Issarti*, J. Rozema, A. Consejo, Corneal modeling and Keratoconus identification, Biomath Commun Suppl 5 (2018).
[43] I. Issarti, A. Consejo, J.J. Rozema, Elevation-based detection of keratoconus, Investig. Ophthalmol. Vis. Sci. 59 (2018) 5810–5810.
[44] P.A. Accardo, S. Pensiero, Neural network-based system for early keratoconus detection from corneal topography, J. Biomed. Inform. 35 (2002) 151–159, https://doi.org/10.1016/S1532-0464(02)00513-0.
[45] Q. Liu, Q. Gu, Z. Wu, Feature selection method based on support vector machine and shape analysis for high-throughput medical data, Comput. Biol. Med. 91 (2017) 103–111, https://doi.org/10.1016/j.compbiomed.2017.10.008.
[46] J. Goldberger, G.E. Hinton, S.T. Roweis, R.R. Salakhutdinov, Neighbourhood components analysis, in: L.K. Saul, Y. Weiss, L. Bottou (Eds.), Adv. Neural Inf. Process. Syst. vol. 17, MIT Press, 2005, pp. 513–520.
[47] F. Cavas-Martínez, L. Bataille, D.G. Fernández-Pacheco, F.J. Cañavate, J.L. Alió, A new approach to keratoconus detection based on corneal morphogeometric analysis, PLoS One 12 (2017) e0184569.
[48] F. Cavas-Martínez, D.G. Fernández-Pacheco, ED la Cruz-Sánchez, J.N. Martínez, F.J.F. Cañavate, A. Vega-Estrada, et al., Geometrical custom modeling of human cornea in vivo and its use for the diagnosis of corneal ectasia, PLoS One 9 (2014) e110249, , https://doi.org/10.1371/journal.pone.0110249.
[49] R. Navarro, J.J. Rozema, M.-J. Tassignon, Optical changes of the human cornea as a function of age, Optom Vis Sci Off Publ Am Acad Optom 90 (2013) 587–598, https://doi.org/10.1097/OPX.0b013e3182928bc6.
[50] M. Belin, J.T. Kim, P. Zloty, R. Ambrósio, A. Barbara, Simplified Nomenclature for Describing Keratoconus, (2012), https://doi.org/10.5005/jp-journals-10025-1006.
[51] G.W. Griffiths, Ł. Płociniczak, W.E. Schiesser, Analysis of cornea curvature using radial basis functions – Part II: fitting to data-set, Comput. Biol. Med. 77 (2016) 285–296, https://doi.org/10.1016/j.compbiomed.2016.06.008.
[52] G.W. Griffiths, Ł. Płociniczak, W.E. Schiesser, Analysis of cornea curvature using radial basis functions – Part I: Methodology, Comput. Biol. Med. 77 (2016) 274–284, https://doi.org/10.1016/j.compbiomed.2016.08.011.
[53] R. Navarro, L. González, J.L. Hernández, Optics of the average normal cornea from general and canonical representations of its surface topography, J Opt Soc Am A Opt Image Sci Vis 23 (2006) 219–232.
[54] A. Martínez-Finkelshtein, D.R. López, G.M. Castro, J.L. Alió, Adaptive cornea modeling from keratometric data, Investig. Ophthalmol. Vis. Sci. 52 (2011) 4963–4970, https://doi.org/10.1167/iovs.10-6774.
[55] M. Schneider*, D.R. Iskander, M.J. Collins, Modeling corneal surfaces with rational functions for high-speed videokeratoscopy data compression, IEEE Trans. Biomed. Eng. 56 (2009) 493–499, https://doi.org/10.1109/TBME.2008.2006019.
[56] M.K. Smolek, S.D. Klyce, Goodness-of-prediction of Zernike polynomial fitting to corneal surfaces, J. Cataract Refract. Surg. 31 (2005) 2350–2355, https://doi.org/10.1016/j.jcrs.2005.05.025.
[57] J. Goldberger, G.E. Hinton, S.T. Roweis, R.R. Salakhutdinov, Neighbourhood components analysis, in: L.K. Saul, Y. Weiss, L. Bottou (Eds.), Adv. Neural Inf. Process. Syst. vol. 17, MIT Press, 2005, pp. 513–520.
[58] W. Yang, K. Wang, W. Zuo, Neighborhood component feature selection for high-dimensional data, J. Comput. 7 (2012), https://doi.org/10.4304/jcp.7.1.161-168.
[59] R. Hecht-Nielsen, Applications of counterpropagation networks, Neural Network. 1

(1988) 131–139, https://doi.org/10.1016/0893-6080(88)90015-9.
[60] D.M. Clark, K. Ravishankar, A convergence theorem for Grossberg learning, Neural Network. 3 (1990) 87–92, https://doi.org/10.1016/0893-6080(90)90047-O.
[61] J.C. Butcher, Numerical Methods for Ordinary Differential Equations, John Wiley & Sons, 2016.
[62] J.C. Butcher, Implicit Runge-Kutta processes, Math. Comput. 18 (1964) 50–64, https://doi.org/10.2307/2003405.
[63] J.C. Butcher, A history of Runge-Kutta methods, Appl. Numer. Math. 20 (1996) 247–260, https://doi.org/10.1016/0168-9274(95)00108-5.
[64] J.C. Butcher, A stability property of implicit Runge-Kutta methods, BIT Numer Math 15 (1975) 358–361, https://doi.org/10.1007/BF01931672.
[65] M.J. Mannis, J. Lightman, R.D. Plotnik, Corneal topography of posterior keratoconus, Cornea 11 (1992) 351–354.
[66] R. Kohavi, A study of cross-validation and bootstrap for accuracy estimation and model selection, Proc. 14th Int. Jt. Conf. Artif. Intell. vol. 2, Morgan Kaufmann Publishers Inc., San Francisco, CA, USA, 1995, pp. 1137–1143.
[67] P.-N. Tan, M. Steinbach, V. Kumar, Introduction to Data Mining, US Ed., Pearson, Boston, 2005.
[68] M. Shajari, I. Jaffary, K. Herrmann, C. Grunwald, G. Steinwender, W.J. Mayer, et al., Early tomographic changes in the eyes of patients with keratoconus, J. Refract. Surg. 34 (2018) 254–259, https://doi.org/10.3928/1081597X-20180124-01.
[69] S. Huseynli, J. Salgado-Borges, J.L. Alio, Comparative evaluation of Scheimpflug tomography parameters between thin non-keratoconic, subclinical keratoconic, and mild keratoconic corneas, Eur. J. Ophthalmol. 28 (2018) 521–534, https://doi.org/10.1177/1120672118760146.
[70] E.S. Hwang, C.E. Perez-Straziota, S.W. Kim, M.R. Santhiago, J.B. Randleman, Distinguishing highly asymmetric keratoconus eyes using combined Scheimpflug and spectral domain OCT analysis, Ophthalmology (2018), https://doi.org/10.1016/j.ophtha.2018.06.020.
[71] M.-R. Sedaghat, H. Momeni-Moghaddam, R. Ambrósio, H.-R. Heidari, N. Maddah, Z. Danesh, et al., Diagnostic ability of corneal shape and biomechanical parameters for detecting frank keratoconus, Cornea 37 (2018) 1025–1034, https://doi.org/10.1097/ICO.0000000000001639.
[72] P. Kosekahya, M. Koc, M. Caglayan, H. Kiziltoprak, C.U. Atilgan, P. Yilmazbas, Repeatability and reliability of ectasia display and topometric indices with the Scheimpflug system in normal and keratoconic eyes, J. Cataract Refract. Surg. 44 (2018) 63–70, https://doi.org/10.1016/j.jcrs.2017.10.042.
[73] D. Smadja, D. Touboul, A. Cohen, E. Doveh, M.R. Santhiago, G.R. Mello, et al., Detection of subclinical keratoconus using an automated decision tree classification, Am. J. Ophthalmol. 156 (2013) 237–246, https://doi.org/10.1016/j.ajo.2013.03.034.
[74] M.C. Arbelaez, F. Versaci, G. Vestri, P. Barboni, G. Savini, Use of a support vector machine for keratoconus and subclinical keratoconus detection by topographic and tomographic data, Ophthalmology 119 (2012) 2231–2238, https://doi.org/10.1016/j.ophtha.2012.06.005.
[75] A. Saad, E. Guilbert, D. Gatinel, Corneal enantiomorphism in normal and keratoconic eyes, J. Refract. Surg. 30 (2014) 542–547, https://doi.org/10.3928/1081597X-20140711-07.
[76] CASSETTE NB Studio, Screening subclinical keratoconus with SCORE Analyzer, Docteur Damien Gatinel n.d. https://www.gatinel.com/recherche-formation/keratocone-2/screening-subclinical-keratoconus-with-score-analyzer/ , Accessed date: 29 January 2019.
[77] B.T. Lopes, I.C. Ramos, M.Q. Salomão, F.P. Guerra, S.C. Schallhorn, J.M. Schallhorn, et al., Enhanced tomographic assessment to detect corneal ectasia based on artificial intelligence, Am. J. Ophthalmol. 195 (2018) 223–232, https://doi.org/10.1016/j.ajo.2018.08.005.
[78] A. Saad, D. Gatinel, Validation of a new scoring system for the detection of early forme of keratoconus, Age 37 (2012) 37–38.
[79] Y. Shi, Strategies for improving the early diagnosis of keratoconus, Clin. Optom. (2016), https://doi.org/10.2147/OPTO.S63486.
[80] A. Martínez-Abad, D.P. Piñero, New perspectives on the detection and progression of keratoconus, J. Cataract Refract. Surg. 43 (2017) 1213–1227, https://doi.org/10.1016/j.jcrs.2017.07.021.
[81] Y.S. Rabinowitz, X. Li, A.L.C. Canedo, R. Ambrósio, Y. Bykhovskaya, Optical coherence tomography combined with videokeratography to differentiate mild keratoconus subtypes, J Refract Surg Thorofare NJ 30 (1995) 80–87, https://doi.org/10.3928/1081597X-20140120-02 2014.
[82] G.H. Bae, J.R. Kim, C.H. Kim, D.H. Lim, E.S. Chung, T.-Y. Chung, Corneal topographic and tomographic analysis of fellow eyes in unilateral keratoconus patients using Pentacam, Am. J. Ophthalmol. 157 (2014), https://doi.org/10.1016/j.ajo.2013.08.014 103-109.e1.

**Prof Jos J. Rozema** currently works at the department of Ophthalmology, Antwerp university hospital Belgium. He is a team leader of the visual optic lab of Antwerp (VOLANTIS) research team. In 2004 he received his first PhD in physics at Antwerp university as well as a second PhD in medical sciences in 2017. Rozema has over 65 research publication over field of clinical research in ophthalmology, eye models, visual optics and machine learning.

**Prof. Carina Koppen** is head of Ophthalmology department at the Antwerp University Hospital, Belgium. Her subspeciality is Cornea, External Eye Disease and Contact Lenses. She is the Medical Director of the Ocular Tissue bank UZA. She defended her PhD in 2012: “Corneal cross-linking and keratoconus”. She has been an invited speaker and course faculty at national and international conferences. She has been an organizer of national and international conferences on cornea, keratoconus, contact lenses and related topics. She is currently the secretary general of the European Contact Lens Society of Ophthalmologists.

**Dr. Alejandra Consejo** received her PhD in Biocybernetics and Biomedical Engineering from Wroclaw University of Science and Technology in 2017. Her doctoral studies focused on modelling the anterior eye morphometry. She received the EYRA 2017 (European Young Researchers Award) as best PhD graduate in Europe. After working one year and a half as postdoc researcher in the Department of Ophthalmology in the Antwerp University Hospital, in Belgium, she joined the Physical Optics & Biophotonics Group to develop a tool based on innovative photonic methods and modelling for the Eye.

**Marta Jiménez-García** is currently a student at Ophthalmology department of Antwerp University hospital. She received her Master's Degree in Advanced Optometry and Vision Sciences in 2017 at the University of Valencia (Spain). She graduated as a Telecommunications Engineer in 2004 at Zaragoza University (Spain) and graduated with the greatest distinction in Optics and Optometry in 2014 at the same university. Her interests are related to the field of Optometry and Optics.

**Sarah Hershko** graduated as a medical doctor in 2018 from the University of Antwerp (UA). She is currently a PhD student at the UA. Her main research and interest areas are straylight and clinical Ophthalmology.

**Issarti ikram** is currently a PhD student in medical sciences at Antwerp University. She received her Master MSc degree in 2016 in Applied Mathematics. Her main interests are related to mathematical modelling and machine learning. She is interested in developing personalized models for disease progression.